

Hole and Electron Doping of Topochemically Reduced Ni(I)/Ru(II) Insulating Ferromagnetic Oxides.

Zheyang Xu, Lun Jin, Julius-Konstantin Backhaus, Felicity Green and Michael A. Hayward*

Department of Chemistry, University of Oxford, Inorganic Chemistry Laboratory, South Parks Road, Oxford, OX1 3QR, UK.

ABSTRACT: $\text{La}_x\text{Sr}_{2-x}\text{NiRuO}_6$, $\text{La}_x\text{Sr}_{4-x}\text{NiRuO}_8$ and $\text{La}_x\text{Sr}_{3-x}\text{NiRuO}_7$ are respectively the $n = \infty$, 1 and 2 members of the $(\text{La}_{x/2}\text{Sr}_{1-(x/2)})_n\text{Sr}(\text{Ni}_{0.5}\text{Ru}_{0.5})_n\text{O}_{3n+1}$ compositional series. Reaction with CaH_2 , in the case of the $\text{La}_x\text{Sr}_{2-x}\text{NiRuO}_6$ perovskite phases, or Zr oxygen-getters in the case of the $\text{La}_x\text{Sr}_{4-x}\text{NiRuO}_8$ and $\text{La}_x\text{Sr}_{3-x}\text{NiRuO}_7$ Ruddlesden-Popper phases, yields the corresponding topochemically reduced $(\text{La}_{x/2}\text{Sr}_{1-(x/2)})_n\text{Sr}(\text{Ni}_{0.5}\text{Ru}_{0.5})_n\text{O}_{3n-1}$ compounds ($\text{La}_x\text{Sr}_{2-x}\text{NiRuO}_4$, $\text{La}_x\text{Sr}_{4-x}\text{NiRuO}_6$ and $\text{La}_x\text{Sr}_{3-x}\text{NiRuO}_5$) which contain Ni and Ru cations in square planar coordination sites. The $x = 1$ members of each series (LaSrNiRuO_4 , $\text{LaSr}_3\text{NiRuO}_6$ and $\text{LaSr}_2\text{NiRuO}_5$) exhibit insulating ferromagnetic behavior at low temperature, attributable to exchange couplings between the Ni^{1+} and Ru^{2+} centers they contain. Increasing the La^{3+} concentration ($x > 1$) leads to a reduction of some of the Ru^{2+} centers to Ru^{1+} centers and a suppression of the ferromagnetic state (lower T_c , reduced saturated ferromagnet moment). In contrast increasing the Sr^{2+} concentration ($x < 1$) oxidizes some of the Ru^{2+} centers to Ru^{3+} centers and enhances the ferromagnetic coupling (increased T_c , increased saturated ferromagnet moment) for the $n = \infty$ and $n = 2$ samples, but appears to have no influence on the magnetic ordering temperature of the $n = 1$ samples. The magnetic couplings and influence of doping is discussed on the basis of super exchange and direct exchange couplings between the square planar Ni and Ru centers.

Introduction

Complex transition-metal oxides exhibit a wide variety of collective, coupled magnetic behaviors, ranging from ‘simple’ ferromagnetic, antiferromagnetic or ferrimagnetic states to coupled properties such as spin-polarized conductivity and magnetoresistance.^{1, 2} This feature of transition-metal oxide chemistry can be attributed to the strong magnetic coupling interactions which exist between transition-metal cations in complex oxides, and the ease with which the strength and sign of these coupling interactions can be modified and tuned by making changes to the chemistry and crystal structures of these systems.

Despite the diverse range of magnetic behaviors exhibited by complex transition-metal oxides, insulating ferromagnetic materials are rather unusual. The rareness of this combination of properties can be explained by noting that cation-cation direct exchange and cation-anion-cation super exchange interactions dominate the magnetic coupling in most insulating oxides, and that the Goodenough-Kanamori rules³ which rationalize the sign of these interactions predict that the coupling between equivalently filled orbitals (i.e. d-orbitals containing the same number of electrons) will be antiferromagnetic. As a result, in the absence of orbital order, self-exchange interactions (i.e. couplings between two identical cations) of this type almost always yield antiferromagnetic states, so the vast majority of insulating transition-metal oxides containing only one type of transition-metal cation are antiferromagnets.

It is possible, in principle, for complex transition-metal oxides to exhibit insulating ferromagnetic behav-

ior on the basis of super exchange coupling, if they contain ordered arrays of two different transition-metal cations with suitable d-orbital fillings. For example, an $\text{A}_2\text{BB}'\text{O}_6$ cation-ordered double perovskite phase containing an ordered arrangement of octahedrally coordinated d^3 , $S = 3/2$ and d^5 , $S = 5/2$ metal centers would have ferromagnetic super exchange couplings between the B and B' cations. However, the preparation of cation ordered perovskite oxides is challenging (cation disordered phases are in general thermodynamically preferred)⁴⁻⁶ and the preparation of cation-ordered perovskite phases with specific d-electron counts even more so.

Low-temperature topochemical reduction allows the preparation of metastable phases, which cannot be prepared via conventional high-temperature synthesis routes, by removing oxide ions from existing complex transition-metal oxide frameworks, in structure-conserving reactions.⁷⁻⁹ This post-synthesis deintercalation of oxide ions allows both the oxidation state and coordination environment of the transition-metal cations in a phase to be modified, while the long-range structure of the materials is maintained.⁹ Recently we reported that the topochemical reduction of the B-site ordered double perovskite LaSrNiRuO_6 yielded the highly metastable phase LaSrNiRuO_4 which contains an ordered array of square-planar coordinated Ni^{1+} and Ru^{2+} cations.¹⁰ On cooling below 250 K, LaSrNiRuO_4 exhibits insulating ferromagnetic behavior, a feature which can be explained on the basis of ferromagnetic exchange interactions between the Ni^{1+} and Ru^{2+} cations.^{10, 11} Here we describe the effects of electronic doping (making small changes to the transition-metal oxidation states) on the magnetic behavior of perovskite-derived LaSrNiRuO_4 and also report

similar ferromagnetic insulating behavior in the analogous $n = 2$ $\text{LaSr}_2\text{NiRuO}_5$, and $n = 1$ $\text{LaSr}_3\text{NiRuO}_6$ topochemically reduced Ruddlesden-Popper phases.

Experimental.

Synthesis of $\text{La}_x\text{Sr}_{2-x}\text{NiRuO}_6$. Samples of $\text{La}_x\text{Sr}_{2-x}\text{NiRuO}_6$ ($0.75 < x < 1.375$) were prepared via a citrate gel method. Suitable stoichiometric ratios of La_2O_3 (99.999%, dried at 900°C), SrCO_3 (99.99%), Ni powder (99.996%), and RuO_2 (99.99% dried at 800°C) were dissolved in a minimum quantity of 6 M nitric acid. 3 mole equivalents of citric acid and 5 ml of analar ethylene glycol were added and the solution was heated with constant stirring. The gels thus formed were subsequently ground into a fine powder, placed in an alumina crucible and heated at 1 °C min⁻¹ to 900 °C in air and held at this temperature for 12 h. The powders were then reground, pressed into 13 mm pellets and then heated at 1200 °C in air for 2 periods of 24 h. After the final heating period samples were rapidly quenched to room temperature in liquid nitrogen.

Synthesis of $\text{La}_x\text{Sr}_{2-x}\text{NiRuO}_4$. Samples of $\text{La}_x\text{Sr}_{2-x}\text{NiRuO}_4$ ($0.85 < x < 1.25$) were prepared by reacting the corresponding $\text{La}_x\text{Sr}_{2-x}\text{NiRuO}_6$ phases with 4 mole equivalents of CaH_2 at 360 °C in a ‘venting’ apparatus described previously.¹² After reaction, calcium containing phases ($\text{CaO} + \text{CaH}_2$) were removed from samples by washing with a 0.05 M solution of NH_4Cl in methanol, and then aliquots of clean methanol, before being dried under vacuum.

Synthesis of $\text{La}_x\text{Sr}_{4-x}\text{NiRuO}_8$. Samples of $\text{La}_x\text{Sr}_{4-x}\text{NiRuO}_8$ ($0.6 < x < 1.4$) were prepared by combining suitable stoichiometric ratios of La_2O_3 (99.999%, dried at 900°C), SrCO_3 (99.994%), RuO_2 (99.99%, dried at 800°C) and NiO (99.998%) in an agate mortar and pestle, transferring the mixtures into an alumina crucible, and then heating at a rate of 1 °C min⁻¹ to 1000 °C in air to decompose the carbonate. Samples were then reground, pressed into pellets and then heated for 3 periods of 48 h at 1200 °C in air, with grinding between heating periods.

Synthesis of $\text{La}_x\text{Sr}_{4-x}\text{NiRuO}_6$. Samples of $\text{La}_x\text{Sr}_{4-x}\text{NiRuO}_6$ ($0.6 < x < 1.4$) were prepared via the reduction of the corresponding $\text{La}_x\text{Sr}_{4-x}\text{NiRuO}_8$ phases with a Zr oxygen getter.⁷ Samples to be reduced were sealed in evacuated silica ampoules along with a glass ‘thimble’ containing 2 mole equivalents of powdered zirconium, such that the two powders shared an atmosphere but were not in physical contact. Samples were heated at 500 °C for 2 periods of 7 d, with samples reground and the Zr replaced between heating periods.

Synthesis of $\text{La}_x\text{Sr}_{3-x}\text{NiRuO}_7$. Samples of $\text{La}_x\text{Sr}_{3-x}\text{NiRuO}_7$ ($x = 0.8, 0.9, 1$) were prepared by combining suitable stoichiometric ratios of La_2O_3 (99.999%, dried at 900°C), SrCO_3 (99.994%), RuO_2 (99.99%, dried at 800°C) and NiO (99.998%) in an agate mortar and pestle, transferring the mixtures into an alumina crucible, and then heating at a rate of 1 °C min⁻¹ to 1000°C in air to decompose the carbonate. Samples were then reground, pressed into pellets and then heated for 4 periods of 48 h at 1250°C in air, with grinding between heating periods.

Synthesis of $\text{La}_x\text{Sr}_{3-x}\text{NiRuO}_5$. Samples of $\text{La}_x\text{Sr}_{3-x}\text{NiRuO}_5$ ($x = 0.8, 0.9, 1$) were prepared via the reduction of the corresponding $\text{La}_x\text{Sr}_{3-x}\text{NiRuO}_7$ phases with a Zr oxygen getter as described above. Samples were heated at

450 °C for 2 periods of 7 d, with samples reground and the Zr replaced between heating periods.

Characterization. Sample purity and reaction progress were monitored by X-ray powder diffraction data which were collected using a PANalytical X’Pert diffractometer incorporating an X’celerator position sensitive detector (monochromatic Cu K α radiation). Data were collected from air sensitive samples under an inert atmosphere using homemade gas-tight sample holders. High-resolution synchrotron X-ray powder diffraction (SXRD) data were collected using instrument I11 at the Diamond Light Source Ltd. SXRD data were collected using Si-calibrated X-rays with an approximate wavelength of 0.825 Å, from samples sealed in 0.3 mm diameter borosilicate glass capillaries. Neutron powder diffraction (NPD) data were collected using the D2B instrument (ILL neutron source, France) from samples sealed under argon and contained within vanadium cans. Rietveld profile refinement was performed using the GSAS suite of programs.¹³ Thermogravimetric measurements were performed by heating powder samples at a rate of 5 °C min⁻¹ under flowing dilute hydrogen or oxygen, using a Mettler-Toledo MX1 thermogravimetric microbalance, and then cooling to 25 °C.

DC magnetization data were collected using a Quantum Design MPMS SQUID magnetometer. Powder samples were loaded into gelatin capsules in an argon-filled glove box, prior to transferring into the cryostat. Data collected at room temperature indicate that samples contain small amounts (< 0.1 wt %) of ferromagnetic Ni, as previously observed for LaSrNiRuO_4 .¹⁰ Therefore magnetization data were collected using a ‘ferromagnetic subtraction’ technique used in the study of LaSrNiRuO_4 , which utilizes the fact that the magnetization of elemental Ni saturates in applied fields greater than 2T, as described in detail the Supporting Information.

Results

Structural characterization of $\text{La}_x\text{Sr}_{2-x}\text{NiRuO}_6$ ($0.75 < x < 1.375$). SXRD data collected from $\text{La}_x\text{Sr}_{2-x}\text{NiRuO}_6$ ($0.75 < x < 1.375$) samples could be indexed using primitive monoclinic unit cells analogous to the reported cell of the $x = 1$ phase, LaSrNiRuO_6 .^{14, 15} Structural models based on the reported Ni/Ru, B-site ordered perovskite structure of LaSrNiRuO_6 (space group $P2_1/n$), but with adjusted La:Sr ratios, were refined against the SXRD data to achieve good fits, indicating single phase samples had been prepared. The refined structural models indicate that all phases exhibit strong Ni:Ru B-site order, with anti-site disorder less than 3(1)% in all cases. Figure 1a shows a plot of the lattice parameters of the $\text{La}_x\text{Sr}_{2-x}\text{NiRuO}_6$ phases as a function of composition, with plots of the diffraction data in the Supporting Information.

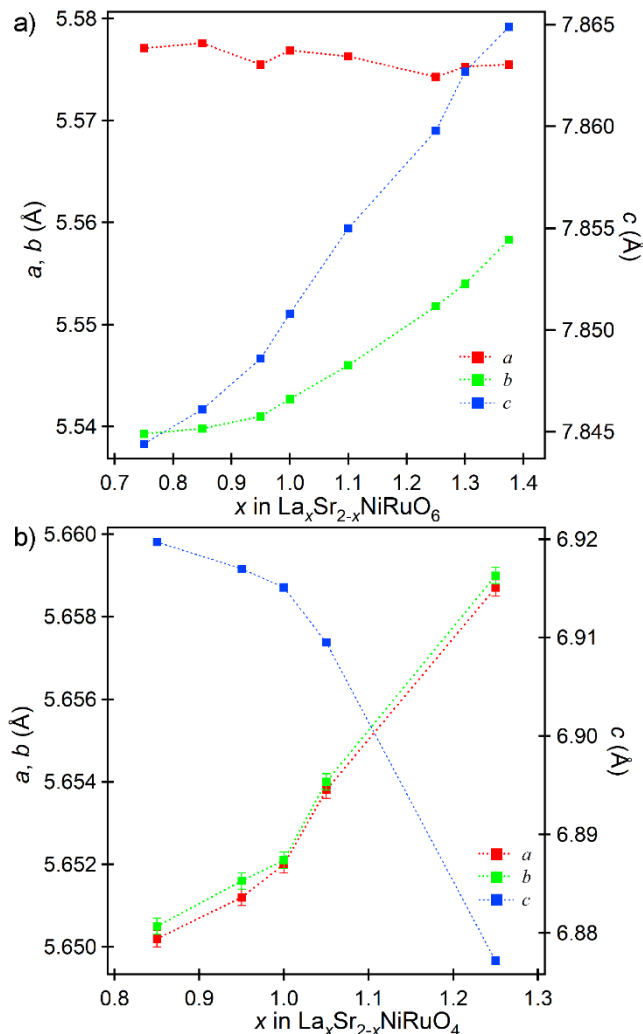


Figure 1. Lattice parameters as a function of composition for a) $\text{La}_x\text{Sr}_{2-x}\text{NiRuO}_6$ and b) $\text{La}_x\text{Sr}_{2-x}\text{NiRuO}_4$ phases.

Structural and chemical characterization of $\text{La}_x\text{Sr}_{2-x}\text{NiRuO}_4$ ($0.85 < x < 1.25$). SXRD data collected from $\text{La}_x\text{Sr}_{2-x}\text{NiRuO}_4$ phases in the composition range $0.85 < x < 1.25$, prepared as described above, could be indexed using body-centered monoclinic cells with lattice parameters similar to those of the $x = 1$ phase, LaSrNiRuO_4 .¹⁰ Reactions between CaH_2 and $\text{La}_{0.75}\text{Sr}_{1.25}\text{NiRuO}_6$ or $\text{La}_{1.375}\text{Sr}_{0.625}\text{NiRuO}_6$ did not yield topochemically reduced products, instead they resulted in partial decomposition to mixtures of La_2O_3 , SrO , Ni and Ru , indicating that only a limited range of $\text{La}_x\text{Sr}_{2-x}\text{NiRuO}_6$ compositions can be reduced to the corresponding $\text{La}_x\text{Sr}_{2-x}\text{NiRuO}_4$ phases. Structural models based on the reported structure of LaSrNiRuO_4 ¹⁰ were refined against the SXRD data from phases in the composition range $0.85 < x < 1.25$ to achieve good fits to the data. Figure 1b shows a plot of the lattice parameters of $\text{La}_x\text{Sr}_{2-x}\text{NiRuO}_4$ phases as a function of composition, with further details and plots of the diffraction data shown in the Supporting Information.

Thermogravimetric data collected while heating samples under 10% H_2 in N_2 , to decompose them to La_2O_3 , SrO , Ni and Ru , are consistent with the stated $\text{La}_x\text{Sr}_{2-x}\text{NiRuO}_4$ sample compositions, within error, as described in detail in the Supporting Information.

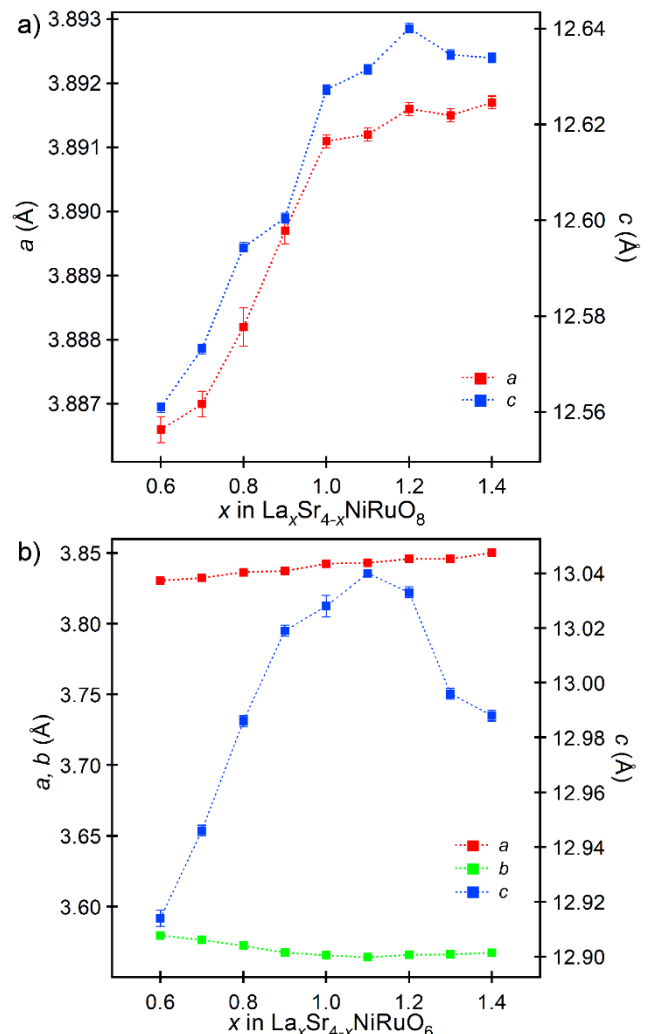


Figure 2. Lattice parameters as a function of composition for a) $\text{La}_x\text{Sr}_{4-x}\text{NiRuO}_8$ and b) $\text{La}_x\text{Sr}_{4-x}\text{NiRuO}_6$ phases.

Structural characterization of $\text{La}_x\text{Sr}_{4-x}\text{NiRuO}_8$ ($0.6 < x < 1.4$). SXRD data collected from $\text{La}_x\text{Sr}_{4-x}\text{NiRuO}_8$ ($0.6 < x < 1.4$) samples could be indexed using body-centered tetragonal unit cells based on the reported structure of the $x = 1$ phase $\text{LaSr}_3\text{NiRuO}_8$.^{16, 17} Structural models based on the reported structure of $\text{LaSr}_3\text{NiRuO}_8$, with adjusted $\text{La}:\text{Sr}$ ratios, were refined against the SXRD data to achieve good fits, indicating single phase samples had been prepared. Figure 2a shows a plot of the lattice parameters of $\text{La}_x\text{Sr}_{4-x}\text{NiRuO}_8$ phases as a function of composition, with further details and plots of the diffraction data shown in the Supporting Information.

Structural and chemical characterization of $\text{LaSr}_3\text{NiRuO}_6$. Thermogravimetric reoxidation data collected from the product of the Zr getter reduction of $\text{LaSr}_3\text{NiRuO}_8$ indicated a composition of $\text{LaSr}_3\text{NiRuO}_{6.00(3)}$ for the reduced phase, as described in the Supporting Information. NPD data collected from $\text{LaSr}_3\text{NiRuO}_6$ could be indexed using a body centered orthorhombic unit cell ($a = 3.8424(1)$ Å, $b = 3.5656(1)$ Å, $c = 13.028(3)$ Å). This combination of composition and lattice parameters are consistent with a topochemically reduced structure for $\text{LaSr}_3\text{NiRuO}_6$ analogous to Sr_2FeO_3 .¹⁸ Thus, a structural model was constructed for $\text{LaSr}_3\text{NiRuO}_6$ based on the structure of Sr_2FeO_3 but with

Atom	x	y	z	Fraction	Uiso (Å ²)
La/Sr	o	o	0.3544(1)	0.25/0.75	0.0086(8)
Ni/Ru	o	o	o	0.5/0.5	0.0121(9)
O (1)	o	o	0.1626(2)	1	0.0126(8)
O (2)	½	o	o	1	0.0193(10)
LaSr ₃ NiRuO ₆ - space group <i>Immm</i> (#71) Formula mass: 657.53 g mol ⁻¹ , Z = 2 <i>a</i> = 3.8424(1) Å, <i>b</i> = 3.5656(1) Å, <i>c</i> = 13.028(3) Å, Volume = 178.49(4) Å ³					
Radiation source: monochromatic neutron λ = 1.5943 Å, 0.8 < d-spacing/Å < 7.5. Temperature: 298 K, ambient pressure. χ^2 = 3.24; wRp = 3.47%; Rp = 3.89%.					

Table 1. Structural parameters from the refinement of LaSr₃NiRuO₆ against NPD data collected at room temperature.

Cation	Anion	length (Å)
La/Sr	O(1)	2.497(3) × 1
	O(1)	2.636(1) × 4
	O(2)	2.606(1) × 2
Ni/Ru	O(1)	2.117(3) × 2
	O(2)	1.924(1) × 2

Table 2. Selected bond lengths from the structure of LaSr₃NiRuO₆ at room temperature.

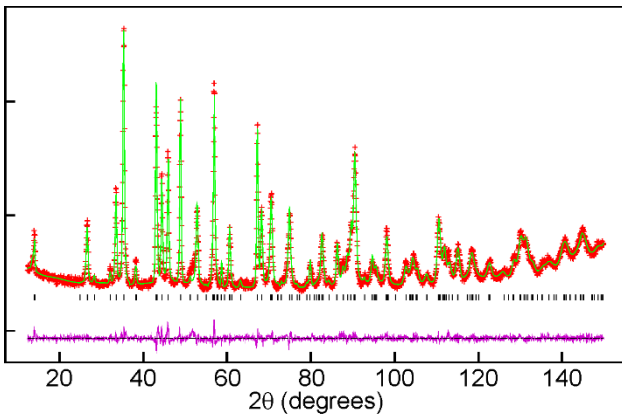


Figure 3. Observed, calculated and difference plots from the structural refinement of LaSr₃NiRuO₆ against powder neutron diffraction data collected at room temperature.

Sr replaced by a disordered 1:3 mixture of La: Sr, and the Fe replaced by a disordered 1:1 mixture of Ni:Ru. This model was refined against the NPD data to achieve a good fit. Full details of the refined structure of LaSr₃NiRuO₆ are given in Table 1, with selected bond lengths in Table 2 and a plot of the observed and calculated diffraction data in Figure 3.

Structural and chemical characterization of La_xSr_{4-x}NiRuO₆ (0.6 < *x* < 1.4). SXR data collected from La_xSr_{4-x}NiRuO₆ samples in the composition range (0.6 < *x* < 1.4) could be indexed using body-centered orthorhombic unit cells with lattice parameters similar to those of the *x* = 1 phase, LaSr₃NiRuO₆. Structural models based on the structure of LaSr₃NiRuO₆ were refined against the SXR data from phases in this composition range, to achieve good fits to the data. Figure 2b shows a

plot of the lattice parameters of La_xSr_{4-x}NiRuO₆ as a function of composition, with further details and plots of the diffraction data shown in the Supporting Information.

Thermogravimetric data collected during the oxidation of La_xSr_{4-x}NiRuO₆ phases back to La_xSr_{4-x}NiRuO₈ are consistent with the stated La_xSr_{4-x}NiRuO₆ compositions.

Structural characterization of La_xSr_{3-x}NiRuO₇ (*x* = 1, 0.9, 0.8). SXR data collected from LaSr₂NiRuO₇ could be indexed using a body-centered tetragonal unit cell with lattice parameters (*a* = 3.9202(1) Å, *c* = 20.3608(2) Å) consistent with an *n* = 2 Ruddlesden-Popper structure analogous to Sr₃Ti₂O₇.¹⁹ A structural model based on Sr₃Ti₂O₇ was constructed with Sr replaced by a disordered 1:2 mixture of La: Sr and Ti replaced by a disordered 1:1 mixture of Ni: Ru, and this model refined against the data to achieve a good fit. Similar structural refinements were performed using SXR data collected from La_{0.9}Sr_{2.1}NiRuO₇ and La_{0.8}Sr_{2.2}NiRuO₇, to achieve good fits. Full details of the refined structures of the La_xSr_{3-x}NiRuO₇ phases are given in the supporting information along with selected bond lengths and plots of the data. Attempts to prepare La_xSr_{2-x}NiRuO₇ phases with *x* > 1 resulted in samples containing mixtures of La_xSr_{2-x}NiRuO₆ perovskite and La_xSr_{4-x}NiRuO₈ *n* = 1 Ruddlesden-Popper impurity phases in addition to the desired *n* = 2 Ruddlesden-Popper phase.

Structural and chemical characterization of La_xSr_{3-x}NiRuO₅ (*x* = 1, 0.9, 0.8). Thermogravimetric re-oxidation data collected from the product of the Zr getter reduction of LaSr₂NiRuO₇ indicated a composition of LaSr₂NiRuO_{5.02(3)} for the reduced phase, as described in the Supporting Information. SXR data collected from LaSr₂NiRuO₅ could be indexed using a body-centered orthorhombic unit cell (*a* = 3.8838(1) Å, *b* = 3.5242(1) Å, *c* = 21.1331(3) Å). This combination of composition and lattice parameters are consistent with a topochemically reduced structure analogous to Sr₃Fe₂O₅.²⁰ Thus, a structural model was constructed for LaSr₂NiRuO₅ based on the structure of Sr₃Fe₂O₅ but with Sr replaced by a 1:2 disordered mixture of La: Sr, and the Fe replaced by a 1:1 disordered mixture of Ni: Ru. This model was refined against the data to achieve a good fit.

Thermogravimetric data indicate compositions of La_{0.9}Sr_{2.1}NiRuO_{5.01(3)} and La_{0.8}Sr_{2.2}NiRuO_{5.01(3)} for the other reduced *n* = 2 Ruddlesden-Popper phases (details in Supporting Information), so similar structural refinements were performed against SXR data collected from the phases. Full details of the refined structures of the La_xSr_{3-x}NiRuO₅ phases are given in the supporting information along with selected bond lengths and plots of the data.

Magnetic characterization of La_xSr_{2-x}NiRuO₄ (0.85 < *x* < 1.25). Magnetization data collected using the ‘ferro-subtraction method’ from La_xSr_{2-x}NiRuO₄ phases (Figure 4) are all qualitatively similar, exhibiting Curie-Weiss behavior at high temperature before a local maximum in

Composition	Curie constant, C ($\text{cm}^3 \text{ K mol}^{-1}$)	Weiss constant, θ (K)	Fitting range (K)	T_c (K)	M_{sat} (μ_B per fu)
$\text{La}_{0.85}\text{Sr}_{1.15}\text{NiRuO}_4$	2.34(2)	+211.2(4)	280 – 300	280(2)	1.21(1)
$\text{La}_{0.95}\text{Sr}_{1.05}\text{NiRuO}_4$	1.75(1)	+207.3(4)	270 – 300	265(2)	1.15(1)
$\text{La}_1\text{Sr}_1\text{NiRuO}_4$	1.39(1)	+192.7(5)	260 – 300	250(2)	1.04(1)
$\text{La}_{1.1}\text{Sr}_{0.9}\text{NiRuO}_4$	1.14(1)	+190.5(4)	260 – 300	240(2)	0.87(1)
$\text{La}_{1.25}\text{Sr}_{0.75}\text{NiRuO}_4$	0.84(2)	+189.8(3)	255 – 300	225(2)	0.67(1)

Table 3. Parameters extracted from the magnetization data from $\text{La}_x\text{Sr}_{2-x}\text{NiRuO}_4$ phases.

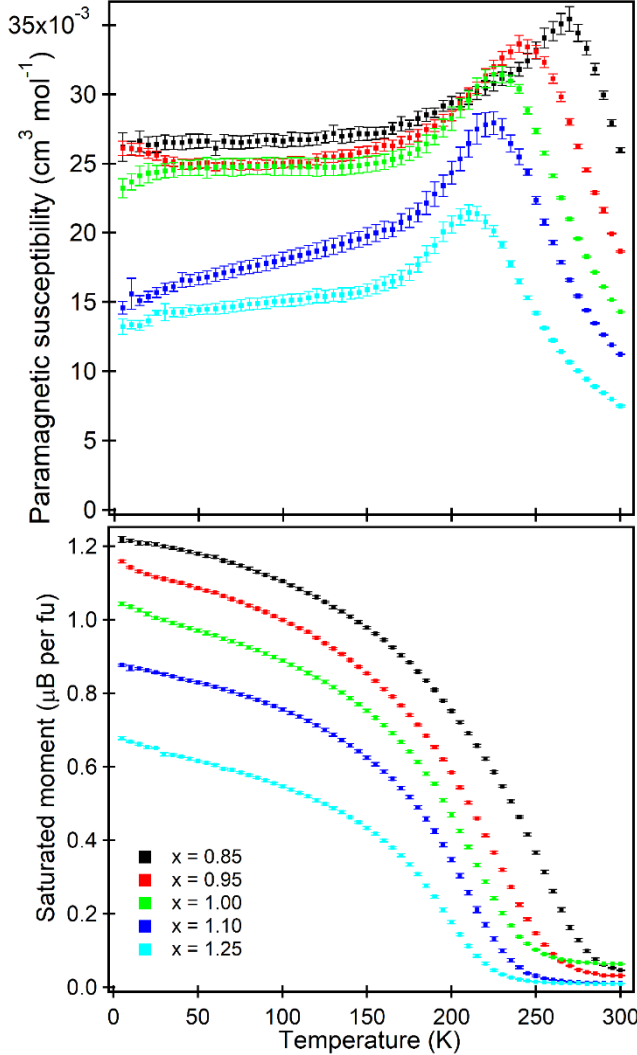


Figure 4. Paramagnetic susceptibility (top) and saturated ferromagnetic moment (bottom) of $\text{La}_x\text{Sr}_{2-x}\text{NiRuO}_4$ phases plotted as a function of temperature.

the paramagnetic susceptibility which coincides with a transition to a ferromagnetic state at low temperature, as previously reported for LaSrNiRuO_4 .¹⁰ Curie-Weiss fits to the high-temperature paramagnetic susceptibility of $\text{La}_x\text{Sr}_{2-x}\text{NiRuO}_4$ phases reveal that both the Curie constant and Weiss temperature decrease with increasing x , as

shown in Table 3 and detailed in the Supporting information. Likewise, the magnetic ordering temperature, T_c (defined as the temperature at which the saturated ferromagnetic moment reaches 5% of its value at 5 K), and the saturated ferromagnetic moment at 5 K also decline with increasing x .

Magnetic characterization of $\text{La}_x\text{Sr}_{4-x}\text{NiRuO}_6$ ($0.7 < x < 1.3$). Magnetization data collected from $\text{LaSr}_3\text{NiRuO}_6$ using the ‘ferro-subtraction method’ (Figure 5) fit the Curie-Weiss law in the range $145 < T/K < 300$ to yield a Curie constant of $1.212(2) \text{ cm}^3 \text{ K mol}^{-1}$ and a Weiss constant of $73.2(5) \text{ K}$ as detailed in the Supporting Information. Below this temperature range there is a transition to a ferromagnetic state analogous to that observed for LaSrNiRuO_4 , which achieves a saturated moment of $\sim 0.6 \mu_B$ per fu at 5 K, confirmed by magnetization-field data shown in the Supporting Information. NPD data collected at 5 K do not show any additional diffraction features compared to analogous data collected at 300 K, which can be attributed to the small size of the ordered moment. However, it should be noted that there is a decline in the low-angle background in the 5 K NPD data, consistent with a decline in paramagnetic scattering associated with the onset of magnetic order. It is possible to refine ferromagnetically ordered magnetic models against the 5 K NPD data with ordered moments of $0.6 \mu_B$ per fu ($0.3 \mu_B$ per transition metal site) to achieve good fits, but the small size of the ordered magnetic moment prevents us from determining the orientation of the magnetic moments relative to the crystallographic axes.

Magnetization data collected from the remaining $\text{La}_x\text{Sr}_{4-x}\text{NiRuO}_6$ samples, using the ‘ferro-subtraction method’, follow the same general form as $\text{LaSr}_3\text{NiRuO}_6$, as shown in Figure 5. However, the Curie and Weiss constants are maximum for the $x = 1$ composition, declining with both increasing and decreasing x , as shown in Table 4 and detailed in the Supporting Information. Similarly, the saturated ferromagnetic moment at 5 K is maximum for the $x = 1$ composition while the ordering temperature, T_c , declines with decreasing x , but remains essentially unchanged with increasing x , as shown in Table 4

Magnetic characterization of $\text{La}_x\text{Sr}_{3-x}\text{NiRuO}_5$ ($x = 1, 0.9, 0.8$). Magnetization data collected from $\text{LaSr}_2\text{NiRuO}_5$ (Figure 6) using the ‘ferro-subtraction method’ adopt the same general form as LaSrNiRuO_4 , following the

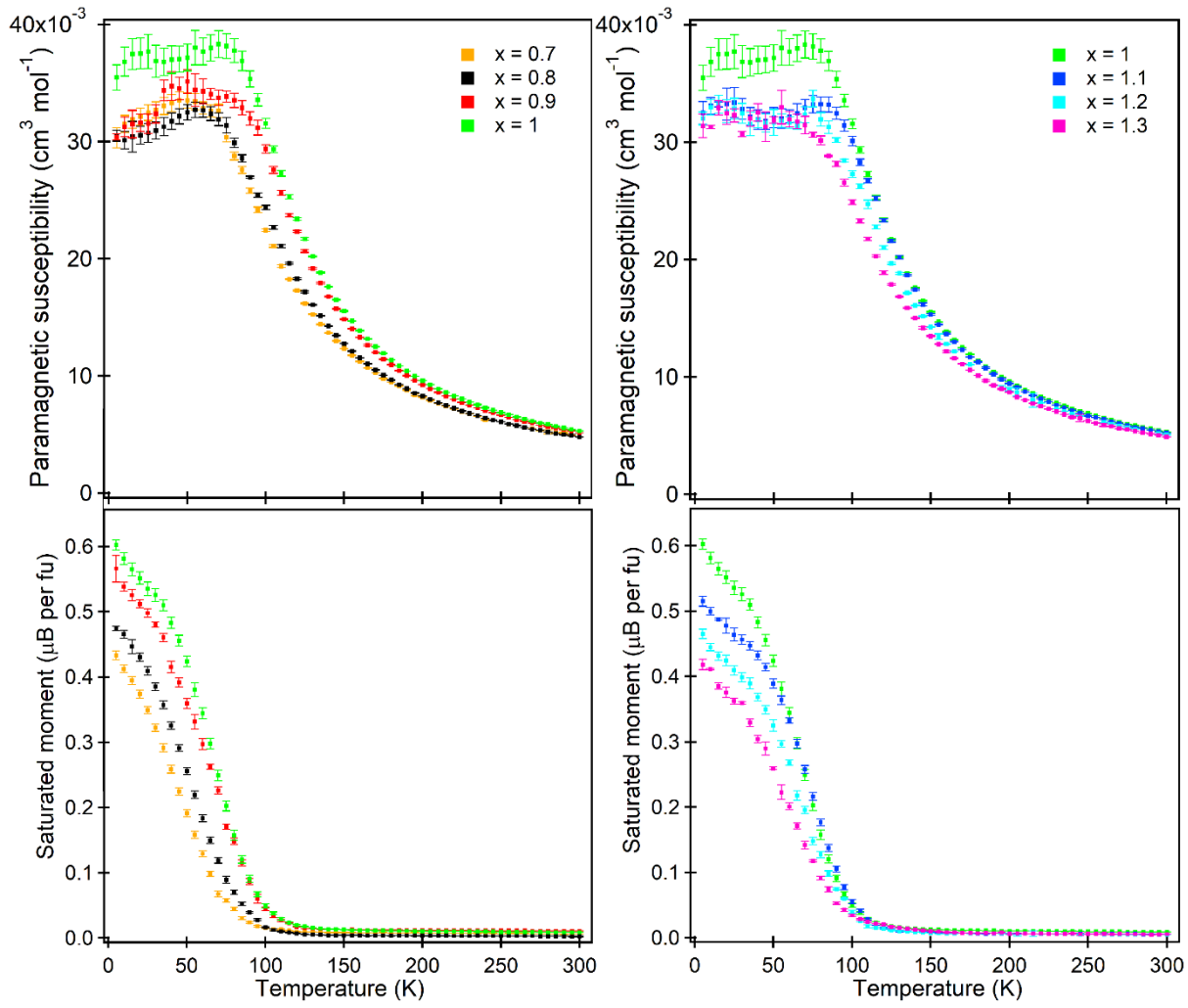


Figure 5. Paramagnetic susceptibility (top) and saturated ferromagnetic moment (bottom) of $\text{La}_x\text{Sr}_{4-x}\text{NiRuO}_6$ phases plotted as a function of temperature.

Composition	Curie constant, C ($\text{cm}^3 \text{ K mol}^{-1}$)	Weiss constant, θ (K)	Fitting range (K)	T_c (K)	M_{sat} (μ_B per fu)
$\text{La}_{0.7}\text{Sr}_{3.3}\text{NiRuO}_6$	1.19(1)	+53.4(3)	120 – 300	85(2)	0.43(1)
$\text{La}_{0.8}\text{Sr}_{3.2}\text{NiRuO}_6$	1.15(1)	+59.7(2)	125 – 300	95(2)	0.47(1)
$\text{La}_{0.9}\text{Sr}_{3.1}\text{NiRuO}_6$	1.20(1)	+69.2(2)	125 – 300	102(2)	0.56(1)
$\text{LaSr}_3\text{NiRuO}_6$	1.22(1)	+71.9(3)	130 – 300	105(2)	0.60(1)
$\text{La}_{1.1}\text{Sr}_{2.9}\text{NiRuO}_6$	1.19(1)	+71.7(2)	130 – 300	106(2)	0.51(1)
$\text{La}_{1.2}\text{Sr}_{2.8}\text{NiRuO}_6$	1.18(1)	+67.0(2)	130 – 300	105(2)	0.46(1)
$\text{La}_{1.3}\text{Sr}_{2.7}\text{NiRuO}_6$	1.15(1)	+65.0(2)	140 – 300	105(2)	0.41(1)

Table 4. Parameters extracted from Curie-Weiss fits to magnetization data from $\text{La}_x\text{Sr}_{4-x}\text{NiRuO}_6$ phases.

Curie-Weiss law in the range $230 < T/\text{K} < 300$ to yield a Curie constant of $1.371(4) \text{ cm}^3 \text{ K mol}^{-1}$ and a Weiss constant of $+166(1) \text{ K}$. Below this temperature range there is a transition to a ferromagnetic state which achieves an ordered-moment of $1.14 \mu_B$ per fu at 5 K, confirmed by magnetization-field data shown in the Supporting Information. In

common with the $\text{La}_x\text{Sr}_{2-x}\text{NiRuO}_4$ phases T_c , the Curie constant, the Weiss constant and the saturated moment at 5 K, all increase with declining x for $\text{La}_x\text{Sr}_{3-x}\text{NiRuO}_5$ phases, as shown in Table 5 and detailed in the Supporting Information.

Composition	Curie constant, C (cm ³ K mol ⁻¹)	Weiss constant, θ (K)	Fitting range (K)	T_c (K)	M_{sat} (μ_B per fu)
LaSr ₂ NiRuO ₅	1.36(1)	+166(1)	230 – 300	200(2)	1.14(1)
La _{0.9} Sr _{2.1} NiRuO ₅	1.46(1)	+173(1)	235 – 300	205(2)	1.36(1)
La _{0.8} Sr _{2.2} NiRuO ₅	1.68(1)	+174(1)	235 – 300	210(2)	1.70(1)

Table 5. Parameters extracted from Curie-Weiss fits to magnetization data from La_xSr_{3-x}NiRuO₅ phases.

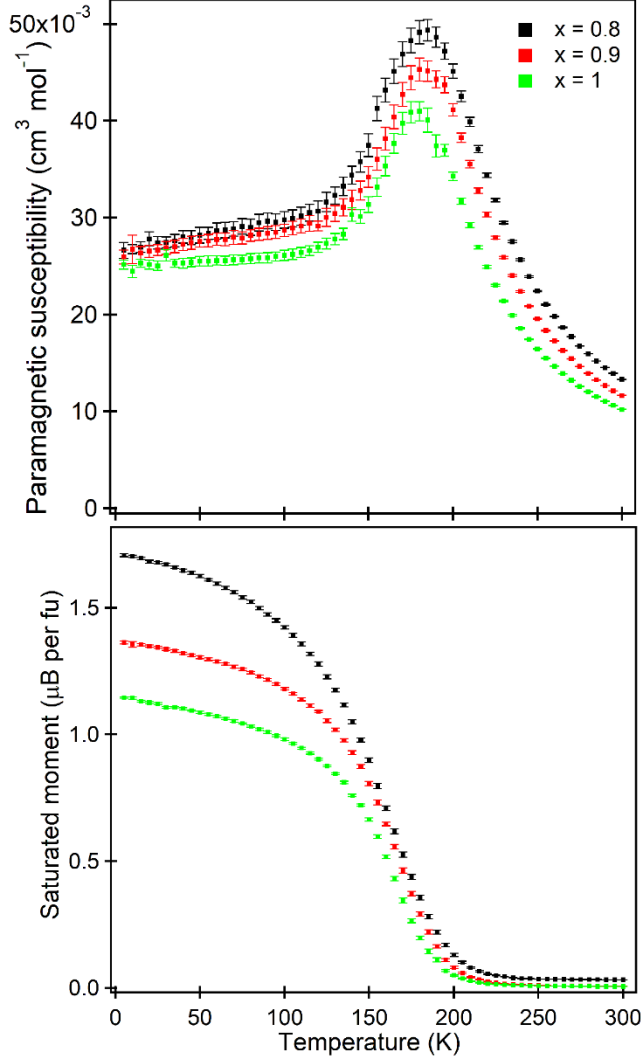


Figure 6. Paramagnetic susceptibility (top) and saturated ferromagnetic moment (bottom) of La_xSr_{3-x}NiRuO₅ phases plotted as a function of temperature.

Discussion

LaSr₃NiRuO₈, LaSr₂NiRuO₇ and LaSrNiRuO₄ are the $n = 1$, $n = 2$ and $n = \infty$ members of the $(\text{La}_{0.5}\text{Sr}_{0.5})_n\text{Sr}(\text{Ni}_{0.5}\text{Ru}_{0.5})_n\text{O}_{3n+1}$ compositional series. LaSrNiRuO₆ adopts a Ni/Ru B-site ordered perovskite structure, as shown in Figure 7a,^{14, 15} while LaSr₃NiRuO₈ and LaSr₂NiRuO₇ adopt $n = 1$ and $n = 2$ Ruddlesden-Popper structures respectively with 2-dimensional, paracrystalline Ni/Ru B-site order, as shown in Figure 7c and 7b respectively.²¹

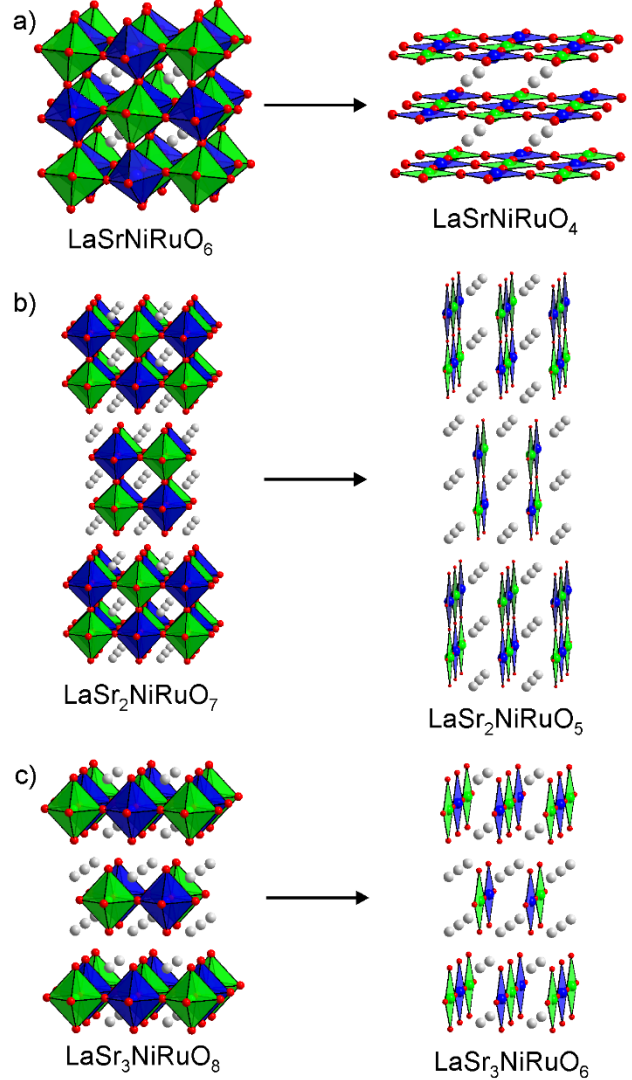


Figure 7. The structures of a) LaSrNiRuO₆ and LaSrNiRuO₄, b) LaSr₂NiRuO₇ and LaSr₂NiRuO₅, and c) LaSr₃NiRuO₈ and LaSr₃NiRuO₆. Grey, green, blue and red spheres represent La/Sr, Ni, Ru and O respectively.

Topochemical reduction converts the $(\text{La}_{0.5}\text{Sr}_{0.5})_n\text{Sr}(\text{Ni}_{0.5}\text{Ru}_{0.5})_n\text{O}_{3n+1}$ phases into the corresponding $(\text{La}_{0.5}\text{Sr}_{0.5})_n\text{Sr}(\text{Ni}_{0.5}\text{Ru}_{0.5})_n\text{O}_{3n-1}$ phases in which the transition-metal cations occupy square-planar coordination sites as shown in Figure 7.

Reactions of the La_xSr_{4-x}NiRuO₈ and La_xSr_{3-x}NiRuO₇ phases reveal that chemical substitution (changing the value of x) does not affect the topochemical reduction

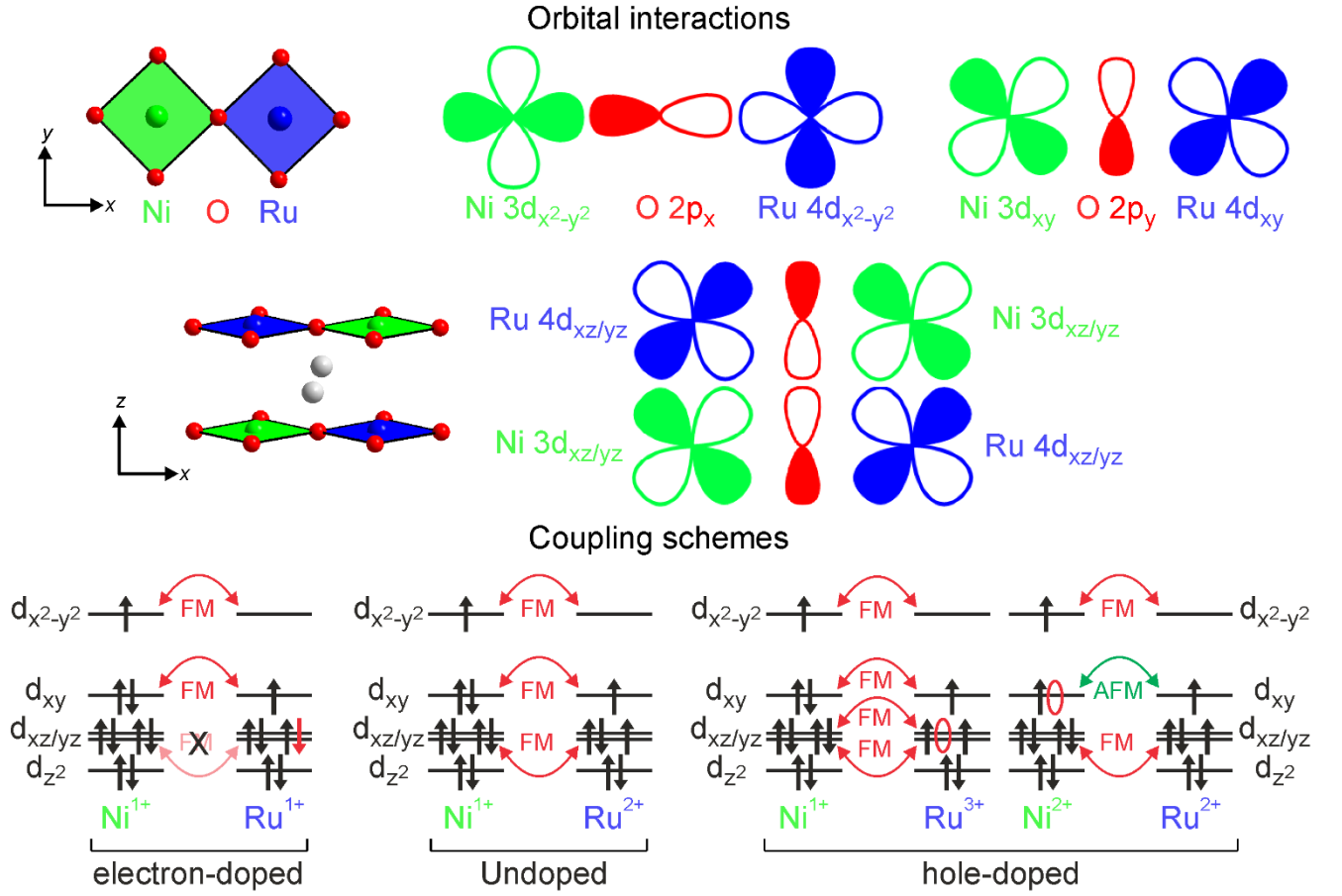


Figure 8. Exchange couplings between Ni and Ru centers in $(\text{La}_{0.5}\text{Sr}_{0.5})_n\text{Sr}(\text{Ni}_{0.5}\text{Ru}_{0.5})_n\text{O}_{3n-1}$ phases

of these materials with Zr oxygen getters, yielding the corresponding $\text{La}_x\text{Sr}_{4-x}\text{NiRuO}_6$ or $\text{La}_x\text{Sr}_{3-x}\text{NiRuO}_5$ compounds for all the compositions prepared.

In contrast the $\text{La}_x\text{Sr}_{2-x}\text{NiRuO}_6$ perovskite phases do not form topochemically reduced products with Zr oxygen getters, and only form topochemically reduced $\text{La}_x\text{Sr}_{2-x}\text{NiRuO}_4$ phases on reaction with CaH_2 for the range $0.85 < x < 1.25$. Similar sensitivity to doping has been observed during the reduction of $\text{SrFeO}_{3-\delta}$ to SrFeO_2 with CaH_2 , where the reduction of lanthanide-doped $\text{Ln}_x\text{Sr}_{1-x}\text{FeO}_{3-\delta}$ phases yield $\text{Ln}_x\text{Sr}_{1-x}\text{FeO}_{2+x/2}$ products rather than $\text{Ln}_x\text{Sr}_{1-x}\text{FeO}_2$, when reacted under the same conditions.^{22, 23}

This differing chemical behavior of the perovskite materials in comparison to the analogous Ruddlesden-Popper phases suggests the La/Sr-O rocksalt sheets within the Ruddlesden-Popper frameworks provide some kinetic stability for the topochemically reduced phases. It should be noted that $\text{La}_x\text{Sr}_{4-x}\text{NiRuO}_8$ and $\text{La}_x\text{Sr}_{3-x}\text{NiRuO}_7$ phases also yield the corresponding $\text{La}_x\text{Sr}_{4-x}\text{NiRuO}_6$ and $\text{La}_x\text{Sr}_{3-x}\text{NiRuO}_5$ materials on reaction with CaH_2 . However, the ease with which these phases are converted to the corresponding $\text{La}_x\text{Sr}_{4-x}\text{NiRuO}_4\text{H}_4$ and $\text{La}_x\text{Sr}_{3-x}\text{NiRuO}_3\text{H}_4$ oxyhydride phases in the presence of CaH_2 makes it hard to isolate pure samples of the anion-deficient compounds by this method, so the Zr getter route is preferred.^{11, 16}

As noted above, the doped phases of LaSrNiRuO_4 , $\text{LaSr}_2\text{NiRuO}_5$ and $\text{LaSr}_3\text{NiRuO}_6$ can be thought of as a series in which the dimensionality of the Ni-O-Ru connectivity

declines from 2D $\text{La}_x\text{Sr}_{2-x}\text{NiRuO}_4$, through intermediate 2D/1D $\text{La}_x\text{Sr}_{3-x}\text{NiRuO}_5$ to 1D $\text{La}_x\text{Sr}_{4-x}\text{NiRuO}_6$. As shown in Figure 7 Magnetization data reveal that the reduced $(\text{La}_{0.5}\text{Sr}_{0.5})_n\text{Sr}(\text{Ni}_{0.5}\text{Ru}_{0.5})_n\text{O}_{3n-1}$ phases undergo transitions to ferromagnetic states at $T_c = 250$ K for LaSrNiRuO_4 ; $T_c = 200$ K for $\text{LaSr}_2\text{NiRuO}_5$ and $T_c = 105$ K for $\text{LaSr}_3\text{NiRuO}_6$. This decline in T_c can be attributed to the reduction in dimensionality from 2D (LaSrNiRuO_4) to 1D ($\text{LaSr}_3\text{NiRuO}_6$). Similar suppression of the magnetic ordering temperatures, i.e. $n = \infty > n = 2$ phases $> n = 1$ phases has been widely observed e.g. SrFeO_2 ($T_N = 468$ K) $> \text{Sr}_3\text{Fe}_2\text{O}_5$ ($T_N = 378$ K) $> \text{Sr}_2\text{FeO}_3$ ($T_N = 179$ K) or SrVO_2H ($T_N > 300$ K) $> \text{Sr}_3\text{V}_2\text{O}_5\text{H}_2$ ($T_N = 240$ K) $> \text{Sr}_2\text{VO}_3\text{H}$ ($T_N = 171$ K)^{20, 22, 24, 25} Transport measurements reveal that all three materials have resistivities in the $\text{M}\Omega\text{cm}$ range, indicating all three phases are rare examples of insulating ferromagnetic materials.

The ferromagnetic behavior of LaSrNiRuO_4 can be explained on the basis of exchange coupling between the cation-ordered $S = 1/2$ Ni^{1+} and intermediate spin-state, $S = 1$ Ru^{2+} centers in the material.^{10, 11, 26} As shown in Figure 8 the intralayer $(\text{Ni}3d_{x^2-y^2})^1\text{-O}2p\text{-(Ru}4d_{x^2-y^2})^0$, $(\text{Ni}3d_{xy})^2\text{-O}2p\text{-(Ru}4d_{xy})^1$ and $(\text{Ni}3d_{xz/yz})^4\text{-O}2p\text{-(Ru}4d_{xz/yz})^3$ super exchange couplings are all ferromagnetic according to the Goodenough-Kanamori rules,³ as is the interlayer $(\text{Ni}3d_{xz/yz})^4\text{-(Ru}4d_{xz/yz})^3$ direct exchange.

Electron-doping of $\text{La}_x\text{Sr}_{2-x}\text{NiRuO}_4$ phases ($x > 1$) leads to a decline in both T_c and the Weiss constant, θ . These changes can be attributed to the partial reduction of $S = 1$,

Ru^{2+} to $S = 1/2$, Ru^{1+} on electron doping as the $(4d_{z^2})^2(4d_{xz/yz})^4(4d_{xy})^1(4d_{x^2-y^2})^0$ configuration of the Ru^{1+} centers would weaken the Ni-Ru ferromagnetic coupling, as shown in Figure 8, consistent with the observed decline in T_c and θ .

Hole-doped samples of LaSrNiRuO_4 exhibit an increase in both T_c and θ . In principle there is an ambiguity over the transition-metal oxidation states in $\text{La}_x\text{Sr}_{2-x}\text{NiRuO}_4$ phases with $x < 1$. Hole doping could oxidize nickel to yield a $\text{Ni}^{1+}/\text{Ru}^{2+}$ combination or oxidize Ru to yield a $\text{Ni}^{1+}\text{Ru}^{2+/3+}$ combination. The partial oxidation of $S = 1/2$, Ni^{1+} to $S = 1$, Ni^{2+} would lead to a weakening of the Ni-Ru magnetic couplings as shown in Figure 8. In contrast, partial oxidation of Ru^{2+} to $S = 3/2$ Ru^{3+} would lead to a strengthening of the Ni-Ru magnetic coupling, consistent with observation, thus the $\text{Ni}^{1+}\text{Ru}^{2+/3+}$ combination is preferred.

Both electron and hole doping of LaSrNiRuO_4 change the filling of the $\text{Ru}4d_{xz/yz}$ orbitals which strongly affects the interlayer Ni-Ru magnetic coupling, which could account for the large changes in T_c observed for doped LaSrNiRuO_4 phases.

The Curie constant, C , obtained for LaSrNiRuO_4 ($1.39(1) \text{ cm}^3 \text{ K mol}^{-1}$) is very close to the value expected for a combination of $S = 1/2$, Ni^{1+} and $S = 1$, Ru^{2+} centers ($1.375 \text{ cm}^3 \text{ K mol}^{-1}$). Electron doping and hole-doping of LaSrNiRuO_4 would be expected to lead to a decrease and increase respectively in the Curie constant of the materials. However, while this trend is observed in the data in Table 3, the measured values of the Curie constant deviate from those expected based on spin-only behavior of $\text{Ni}^{1+}\text{Ru}^{1+/2+}$ or $\text{Ni}^{1+}\text{Ru}^{2+/3+}$ combinations, indicating doped samples do not exhibit simple paramagnetic behavior above T_c .

Previously we had suggested, on the basis of NPD and magnetization data, that LaSrNiRuO_4 could undergo a ruthenium spin-state transition coincident with the onset of ferromagnetic order.¹⁰ The observation that hole-doped $\text{La}_x\text{Sr}_{2-x}\text{NiRuO}_4$ phases exhibit saturated ferromagnetic moments greater than $1 \mu_B$ per fu is incompatible with this proposal.

The intermediate 2D/1D phase $\text{LaSr}_2\text{NiRuO}_5$ exhibits magnetic behavior analogous to that of LaSrNiRuO_4 , albeit with a lower value of T_c (200 K) for the $n = 2$ phase. The Curie constant ($1.36(1) \text{ cm}^3 \text{ K mol}^{-1}$) extracted for $\text{LaSr}_2\text{NiRuO}_5$ from data above 230 K is consistent with the presence of Ni^{1+} and Ru^{2+} , thus the low-temperature ferromagnetic behavior observed for $\text{LaSr}_2\text{NiRuO}_5$ can also be explained by the coupling scheme used for LaSrNiRuO_4 , shown in Figure 8. Likewise, the increase in T_c , θ and C on hole doping ($\text{La}_x\text{Sr}_{3-x}\text{NiRuO}_5$ with $x < 1$) can be accounted for in same way as hole-doped $\text{La}_x\text{Sr}_{2-x}\text{NiRuO}_4$ phases.

The 1D phase $\text{LaSr}_3\text{NiRuO}_6$ also becomes ferromagnetic at low temperature, but there are a number of subtle differences between the magnetic behavior of the $n = 1$ phases and that of LaSrNiRuO_4 and $\text{LaSr}_2\text{NiRuO}_5$. Firstly the Curie constant of $\text{LaSr}_3\text{NiRuO}_6$ ($1.22(1) \text{ cm}^3 \text{ K mol}^{-1}$) is smaller than expected for a combination of $S = 1/2$, Ni^{1+} and $S = 1$, Ru^{2+} and shows only a very small variation with hole or electron doping. In addition, the saturated ferromagnetic moment at 5 K of $\text{La}_x\text{Sr}_{4-x}\text{NiRuO}_6$ materials is about half the

size of the corresponding perovskite and $n = 2$ phases. Finally, Table 4 reveals that hole doping of $\text{LaSr}_3\text{NiRuO}_6$ leads to a decline in T_c and θ , while electron doping doesn't appear to change T_c but leads to a modest decline in θ .

The structural and chemical similarity of the $n = 1$ $\text{La}_x\text{Sr}_{4-x}\text{NiRuO}_6$ phases and the perovskite $\text{La}_x\text{Sr}_{2-x}\text{NiRuO}_4$ and $n = 2$ $\text{La}_x\text{Sr}_{3-x}\text{NiRuO}_5$ phases mean that it is likely that the ferromagnetic behavior observed for $n = 1$ phases also derives from super exchange interactions between square-planar Ni^{1+} and Ru^{2+} centers. However, it is hard to explain the effects of electron and hole-doping on the magnetic behavior of the $n = 1$ phases using simple super exchange arguments.

As noted above the presence of the rock salt layers in the structures of Ruddlesden-Popper phases leads to a lowering of magnetic ordering temperatures compared to perovskite analogues. This explains the depressed T_c of $\text{LaSr}_3\text{NiRuO}_6$ ($T_c = 105 \text{ K}$) compared LaSrNiRuO_4 , and this weakening of magnetic interactions along the z-axis also provides an explanation for the reduced saturated moments observed for $\text{La}_x\text{Sr}_{4-x}\text{NiRuO}_6$ phases.

The reduced dimensionality of the $n = 1$ phases could also be responsible for the doping effects. Figure 7 shows that removal of oxide ions from $\text{La}_x\text{Sr}_{2-x}\text{NiRuO}_6$ phases yields a phase with 2-dimensional Ni-O-Ru connectivity. In contrast, reduction of $\text{La}_x\text{Sr}_{4-x}\text{NiRuO}_8$ yields phases with 1-dimensional Ni-O-Ru connectivity, with the dimensionality of reduced $\text{La}_x\text{Sr}_{3-x}\text{NiRuO}_5$ phases being intermediate between these two values. This lower dimensionality means that 'interlayer' couplings along the z-axis, which do not arise from simple super exchange interactions, can dominate the magnetic behavior of the $n = 1$ phases. In addition, the cleaving of the Ni-O-Ru connectivity into 1D chains means $\text{La}_x\text{Sr}_{4-x}\text{NiRuO}_6$ phases have no Ru-O-O-Ru or Ni-O-O-Ni next-nearest neighbor couplings which may be important. Further study and computation will be required to fully analyze these features of the magnetic behavior.

Conclusion

Topochemical reduction of Ni-Ru cation-ordered $(\text{La}_{0.5}\text{Sr}_{0.5})_n\text{Sr}(\text{Ni}_{0.5}\text{Ru}_{0.5})_n\text{O}_{3n+1}$ perovskite phases yields compounds of composition $(\text{La}_{0.5}\text{Sr}_{0.5})_n\text{Sr}(\text{Ni}_{0.5}\text{Ru}_{0.5})_n\text{O}_{3n-1}$ consisting of ordered arrays of Ni^{1+} and Ru^{2+} cations in square-planar coordination environments. The electron counts and spin states of the transition-metal cations are such that Ni-Ru magnetic exchange interactions lead to ferromagnetic states at low temperature, despite the insulating nature of these phases. This demonstrates the utility of post-synthetic topochemical modification of complex oxides to prepare compounds with unusual combinations of long-range crystal structure and metal oxidation state, which cannot be easily prepared by conventional high-temperature synthesis routes. The apparent insensitivity of the anion deintercalation reactions to electronic doping of the $n = 1$ and $n = 2$ Ruddlesden-Popper phases suggests that the electronic behavior of some topochemically reduced phases can be fine-tuned via cation substitution, in an analogy to the strategy very successfully employed in the large number of materials prepared under thermodynamic control.

ASSOCIATED CONTENT

Supporting Information. Detailed descriptions of the structural, chemical and magnetic characterization of $\text{La}_x\text{Sr}_{2-x}\text{NiRuO}_6$, $\text{La}_x\text{Sr}_{2-x}\text{NiRuO}_4$, $\text{La}_x\text{Sr}_{4-x}\text{NiRuO}_8$, $\text{La}_x\text{Sr}_{4-x}\text{NiRuO}_6$, $\text{La}_x\text{Sr}_{3-x}\text{NiRuO}_7$ and $\text{La}_x\text{Sr}_{3-x}\text{NiRuO}_5$. Description of the ‘ferrosubtraction’ method used to measure the magnetization of reduced samples.

AUTHOR INFORMATION

Corresponding Author

* michael.hayward@chem.ox.ac.uk

Author Contributions

The manuscript was written through contributions of all authors.

ACKNOWLEDGMENT

Experiments at the Diamond Light Source were performed as part of the Block Allocation Group award “Oxford Solid State Chemistry BAG to probe composition-structure-property relationships in solids” (EE13284). We thank E. Suard for assistance collecting neutron diffraction data at the ILL facility.

REFERENCES

1. Goodenough, J. B., *Localized to itinerant electronic transition in perovskite oxides*. Springer-Verlag: Berlin, 2001.
2. Tilley, R. J. D., *Perovskites: Structure-Property Relationships*. John Wiley and Sons: Chichester 2016.
3. Goodenough, J. B., *Magnetism and the chemical bond*. Wiley: New York, 1963.
4. Anderson, M. T.; Greenwood, K. B.; Taylor, G. A.; Poeppelmeier, K. R., B-cation arrangements in double perovskites. *Prog. Solid St. Chem.* **1993**, *22*, 197-233.
5. King, G.; Woodward, P. M., Cation Ordering in Perovskites. *J. Mater. Chem.* **2010**, *20*, 5785-5796.
6. Vasala, S.; Karppinen, M., $\text{A}_2\text{B}'\text{B}''\text{O}_6$ perovskites: a review. *Prog. Solid St. Chem.* **2015**, *43* (1-2), 1-36.
7. Hayward, M. A., Soft chemistry synthesis of oxides. In *Comprehensive Inorganic Chemistry II*, Reedijk, J.; Poeppelmeier, K. R., Eds. Elsevier: Oxford, 2013; Vol. 2, pp 417-453.
8. Hayward, M. A., Topochemical Reactions of Layered Transition-Metal Oxides. *Semiconductor Science and Technology* **2014**, *29* (6), 64010.
9. Hayward, M. A., Synthesis and Magnetism of Extended Solids Containing Transition-Metal Cations in Square-Planar, MO_4 Coordination Sites. *Inorg. Chem.* **2019**, *58* (18), 11961-11970.
10. Amano Patino, M.; Zeng, D.; Bower, R.; McGrady, J. E.; Hayward, M. A., Coupled electronic and magnetic phase transition in the infinite-layer phase LaSrNiRuO_4 . *Inorg. Chem.* **2016**, *55* (17), 9012-9016.
11. Zhu, S. S.; Fan, F. R.; Yang, K.; Wu, H., Ferromagnetism in the unusual low-valence layered material LaSrNiRuO_4 . *Epl* **2017**, *117* (3).
12. O'Malley, M.; Lockett, M. A.; Hayward, M. A., Anion vacancy ordering in $\text{Sr}_7\text{Mn}_4\text{O}_{15-x}$ phases. *J. Solid State Chem.* **2007**, *180*, 2851-2858.
13. Larson, A. C.; Von Dreele, R. B. *General Structure Analysis System*, Los Alamos National Laboratory Report LAUR 86-748: 2000.
14. Gateshki, M.; Igartua, J. M., Crystal structures and phase transitions of the double perovskite oxides SrLaCuRuO_6 and SrLaNiRuO_6 . *Mater. Res. Bull.* **2003**, *38* (14), 1893-1900.
15. Morrow, R.; McGuire, M. A.; Yan, J. Q.; Woodward, P. M., The Crystal Structure and Magnetic Behavior of Quinary Osmate and Ruthenate Double Perovskites $\text{LaAB}'\text{B}''\text{O}_6$ ($\text{A} = \text{Ca}$, Sr ; $\text{B} = \text{Co}$, Ni ; $\text{B}' = \text{Ru}$, Os). *Inorg. Chem.* **2018**, *57* (6), 2989-3001.
16. Jin, L.; Lane, M.; Zeng, D.; Kirschner, F. K. K.; Lang, F.; Manuel, P.; Blundell, S. J.; McGrady, J. E.; Hayward, M. A., $\text{LaSr}_3\text{NiRuO}_4\text{H}_4$: a 4d transition-metal oxide-hydride containing metal hydride sheets. *Angew. Chem., Int. Ed.* **2018**, *57*, 5025-5028.
17. Jin, L.; Hayward, M. A., Hole and Electron Doping of the 4d Transition-Metal Oxyhydride $\text{LaSr}_3\text{NiRuO}_4\text{H}_4$. *Angew. Chem., Int. Ed.* **2020**, *59* (5), 2076-2079.
18. Tassel, C.; Seiberg, L.; Hayashi, N.; Ganesanpotti, S.; Ajiro, Y.; Kobayashi, Y.; Kageyama, H., Sr_2FeO_3 with Stacked Infinite Chains of FeO_4 Square Planes. *Inorg. Chem.* **2013**, *52* (10), 6096-6102.
19. Ruddlesden, S. N.; Popper, P., The compound $\text{S}_3\text{Ti}_2\text{O}_7$ and its structure. *Acta Cryst.* **1958**, *11*, 54-55.
20. Kageyama, H.; Watanabe, T.; Tsujimoto, Y.; Kitada, A.; Sumida, Y.; Kanamori, K.; Yoshimura, K.; Hayashi, N.; Muranaka, S.; Takano, M.; Ceretti, M.; Paulus, W.; Ritter, C.; Andre, G., Spin-ladder iron oxide $\text{Sr}_3\text{Fe}_2\text{O}_5$. *Angew. Chem.* **2008**, *47*, 5740-5745.
21. Robinson, M. L.; Whitaker, E.; Jin, L.; Hayward, M. A.; Laurita, G., Evidence of Paracrystalline Cation Order in the Ruddlesden-Popper Phase $\text{LaSr}_3\text{NiRuO}_8$ through Neutron Total Scattering Techniques. *Inorg. Chem.* **2020**, *59* (5), 3026-3033.
22. Tsujimoto, Y.; Tassel, C.; Hayashi, N.; Watanabe, T.; Kageyama, H.; Yoshimura, K.; Takano, M.; Ceretti, M.; Ritter, C.; Paulus, W., Infinite-layer iron oxide with a square-planar coordination. *Nature* **2007**, *450*, 1062-1065.
23. Yamamoto, T.; Ohkubo, H.; Tassel, C.; Hayashi, N.; Kawasaki, S.; Okada, T.; Yagi, T.; Hester, J.; Avdeev, M.; Kobayashi, Y.; Kageyama, H., Impact of lanthanoid substitution on the structural and physical properties of an infinite-layer iron oxide. *Inorg. Chem.* **2016**, *55* (22), 12093-12099.
24. Denis Romero, F.; Leach, A.; Moller, J. S.; Foronda, F.; Blundell, S.; Hayward, M. A., Strontium vanadium oxide-hydrides: ‘square-planar’ two-electron phases. *Angew. Chem., Int. Ed.* **2014**, *53*, 7556-7559.
25. Tassel, C.; Pruneda, J. M.; Hayashi, N.; Watanabe, T.; Kitada, A.; Tsujimoto, Y.; Kageyama, H.; Yoshimura, K.; Takano, M.; Nishi, M.; Ohoyama, K.; Mizumaki, M.; Kawamura, N.; Iniguez, J.; Canadell, E., CaFeO_2 : A New Type of Layered Structure with Iron in a Distorted Square Planar Coordination. *J. Am. Chem. Soc.* **2009**, *131* (1), 221-229.
26. Denis Romero, F.; Burr, S. J.; McGrady, J. E.; Gianolio, D.; Cibin, G.; Hayward, M. A., $\text{SrFe}_{0.5}\text{Ru}_{0.5}\text{O}_2$: Square-planar Ru^{2+} in an extended oxide. *J. Am. Chem. Soc.* **2013**, *135* (5), 1838-1844.

SYNOPSIS TOC.

Topochemical reduction of Ni/Ru ordered perovskite and Ruddlesden-Popper oxides yields reduced phases containing ordered arrays of Ni^{1+} and Ru^{2+} centers in square-planar coordination environments. Magnetization data indicate these reduced phases exhibit insulating ferromagnetic behavior at low temperature which can be tuned via *A*-site cation substitution.

For Table of Contents only:

